Field Testing of Feedforward Collective Pitch Control on the CART2 Using a Nacelle-Based Lidar Scanner

David Schlipf[1], Paul Fleming[2], Florian Haizmann[1], Andrew Scholbrock[2], Martin Hofsäß[1], Alan Wright[2] and Po Wen Cheng[1]

[1] Stuttgart Wind Energy Research (SWE), Universität Stuttgart, Germany,
[2] National Renewable Energy Laboratory (NREL), USA

E-mail:
[1] David.Schlipf/Florian.Haizmann/Martin.Hofsaess/PoWen.Cheng@ifb.uni-stuttgart.de
[2] Paul.Fleming/Andrew.Scholbrock/Alan.Wright@nrel.gov

Abstract. This work presents the results from a field test of LIDAR assisted collective pitch control using a scanning LIDAR device installed on the nacelle of a mid-scale research turbine. A nonlinear feedforward controller is extended by an adaptive filter to remove all uncorrelated frequencies of the wind speed measurement to avoid unnecessary control action. Positive effects on the rotor speed regulation as well as on tower, blade and shaft loads have been observed in the case that the previous measured correlation and timing between the wind preview and the turbine reaction are accomplish. The feedforward controller had negative impact, when the LIDAR measurement was disturbed by obstacles in front of the turbine. This work proves, that LIDAR is valuable tool for wind turbine control not only in simulations but also under real conditions. Furthermore, the paper shows that further understanding of the relationship between the wind measurement and the turbine reaction is crucial to improve LIDAR assisted control of wind turbines.

1. Introduction

LIDAR (LIght Detection And Ranging) systems are able to provide information about the wind field approaching a wind turbine in advance, which can be used to assist wind turbine control. While early work on LIDAR-assisted control was made by [1], this field of investigations has increased significantly in recent years, and several feedforward and model predictive controllers have been proposed for load reduction or increasing the energy yield, see e.g., [2]-[7]. The feedforward collective pitch control as proposed in [8] has the advantage, that it can be implemented as a simple update to existing feedback controllers. The controller can be combined with an adaptive filter to account for the changes in the correlation and the timing between the LIDAR measurement and the turbine reaction due to changes in the mean wind speed [9]. This work presents the results and experience from a field test to proof the concept under real conditions, using a scanning LIDAR device installed on the nacelle of the CART2 (Controls Advanced Research Turbine, 2-Bladed, [10]) turbine at NREL.

   This paper is organized as follows. Section 2 summarizes the experimental environment. In Section 3 the LIDAR sensing process and the used controller are outlined. The correlation of the LIDAR and the turbine is described in Section 4. Section 5 presents the measured results and a simulation study based on the data. Conclusions and future work are discussed in Section 6.

2. Test Environment

In this section the test site, turbine and LIDAR system for the field testing are described.

2.1. Test Site

The field testing took place at the National Wind Technology Center (NWTC) in Boulder, Colorado, which is part of the National Renewable Energy Laboratory (NREL). Due to its location directly in front of the Rocky Mountains Front Range NWTC offers good conditions during the wind season in winter to perform any kind of field test. Since the wind conditions are rather gusty and extreme, especially tests under extreme conditions can be performed there.

2.2. Test Turbine

Among several multi-megawatt turbines, the NWTC owns two mid-sized turbines, which are dedicated to the testing of new and advanced control algorithms of wind turbines, the so-called Controls Advanced Research Turbines (CARTs). These two turbines are two 600 kW Westinghouse *WTG-600* turbines, which were originally deployed in a wind farm on Hawaii. The CART2 (Figure 1a) is still equipped with the original two-bladed rotor, but was retrofitted with high-speed electromechanical pitch drives, a new fully controllable power electronics, and is heavily instrumented with strain gauges, accelerometers, as well as a dedicated meteorological tower, installed 80 m in front of the turbine in mean wind direction (292°). The turbine has a rotor diameter of $D = 42.7$ m at a hub height of 36.9 m and runs at a rated rotor speed of 41.7 rpm. Since it is a two-bladed turbine, it has a teetered hub, which was free during the test runs. Furthermore, a control system was developed and implemented in LabVIEW by NWTC engineers. This control system runs as a 400 Hz real-time system, which needs to be supervised by an engineer. Although, it handles all possible operating failures, an unattended run of this test turbine is not yet possible. However, it offers engineers an easy way of implementing their own controller code as a DLL, which is then loaded by the LabVIEW framework control system. For this work the DLL was created as an export from MATLAB/Simulink code.
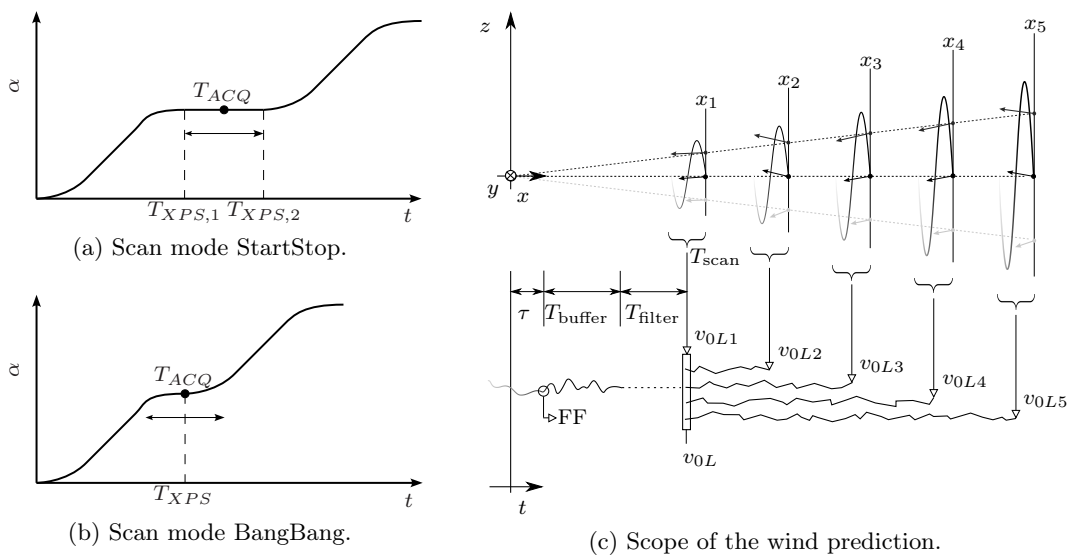
2.3. Used LIDAR System

A scanning LIDAR system [11] from the University of Stuttgart was installed on the CART2 in early 2012. It was placed on a frame which was mounted on the front top of the railing of the platform on top of the CART2's nacelle, as it can be seen in Figure 1b. To compensate the 3.77° tilt of the CART2 nacelle, the LIDAR was mounted with a counter angle of about 3.7°, so that the system itself is horizontal aligned.

The system consists of two parts: A Windcube V1 from *Leosphere* and a scanner unit developed at the University of Stuttgart. Since the original Windcube was designed for site assessment with its beam pointing upwards, a two-degrees-of-freedom mirror for redirecting the beam in any position within the mirror's range was installed in a second casing, which allows pointing sideways. The accessible area is a $0.75D$ x $0.75D$ square in $1D$ distance. Figure 1c shows a picture of the scanner's mirror and the side window through which the laser beam emits. A modified software synchronizes the laser with the two motor stages. This software allows in principle a free design of the scanning trajectories within the mechanical constrains, but in this campaign only two different scanning modes were used: In the "StartStop" mode (see Figure 2a) the center of the acquisition time T_{ACQ} is centered between two stop times T_{XPS}. In the "BangBang" mode (see Figure 2b) the center of the acquisition time T_{ACQ} coincides with one stop time T_{XPS} to be faster than the "StartStop" mode but to distribute the measurement over a small angle α. The LIDAR raw data are the line-of-sight wind speed v_{los}, the Carrier to Noise Ratio (CNR), the two angular positions of the motors, the focus length along the beam for each focus distance and the times T_{ACQ} and T_{XPS}. The modified software allows to use up to 5 scan distances (see Figure 2c).

(a) The CART2.

(b) The SWE-LIDAR installed on the CART2.

(c) Two-DOF mirror seen from internal webcam.

Figure 1. Test environment at NREL.

(a) Scan mode StartStop.

(b) Scan mode BangBang.

(c) Scope of the wind prediction.

Figure 2. Scan of the wind inflow.

3. Controller Design

This section gives a short overview of the reconstruction of the rotor effective wind speed from the LIDAR data and the feedback and feedforward controller. Implementation issues are also addressed.

3.1. Feedback Controller

The baseline feedback controller is a slightly modified standard wind turbine controller. The torque controller uses a normal $k\Omega_g^2$ law in region 2 and a constant torque is applied in region 3. The pitch controller is called a PI/ID type controller, which is a PI controller with an additional integrated derivative term. The design and motivation for this control law are provided in [12]. In practice, the controller performs similarly to a normal PI controller. Both the torque and pitch controller follow the standard practice of feeding back only the generator speed term for control. The controller includes several additional elements including roll-off filters, notch filters on certain resonance and disturbance frequencies, and finally a tower-resonance avoidance scheme. The baseline controller is used as a reference in a number of past studies. For example, it is used as the base controller with which to compare a state-space IPC controller in [13].

3.2. LIDAR Preview

For this campaign circular trajectories, with 6 focus points in 5 focus distances equally distributed between $x_1 = 1D = 42.7\,\mathrm{m}$ and $x_5 = 2D = 85.3\,\mathrm{m}$ (see Figure 2c) were used. The duration of one scan is for the "BangBang" mode $T_{Scan} = 1.33\,\mathrm{s}$ and for the "StartStop" mode $T_{Scan} = 2.42\,\mathrm{s}$. For the acquisition of one measurement 2000 pulses with an average duration of $0.144\,\mathrm{s}$ are used. For each distance j, data points with bad synchronization or low CNR (see Section 4) are removed. For the remaining data points the longitudinal wind component is reconstructed assuming lateral and vertical wind components to be zero and by averaging over the last trajectory

$$v_{0Lj}(t) = \frac{1}{6} \sum_{i=1}^{6} v_{los,ij}/l_{xi}, \tag{1}$$

where l_{xi} is the laser vector component in inflow wind direction. The obtained time series v_{0Lj} is time-shifted according to Taylor's frozen turbulence hypothesis (see Figure 2c), which assumes that the turbulent wind field moves with the average wind speed: The time to reach the first focus distance is assumed to be $(x_j - x_1)/\bar{v}$, where $\bar{v}$ is the mean wind speed. The LIDAR estimate of the rotor effective wind speed $v_{0L}(t)$ is then calculated by
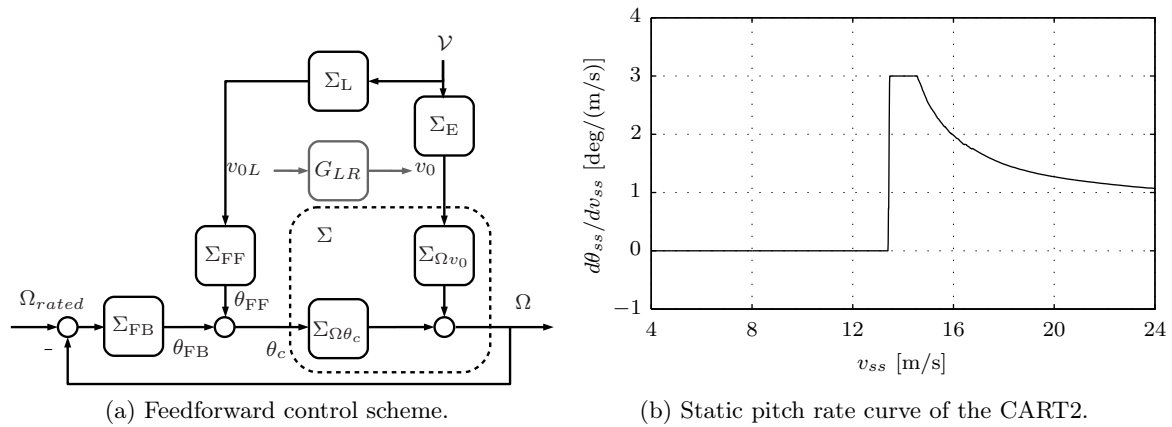
$$v_{0L}(t) = \frac{1}{5} \sum_{j=1}^{5} v_{0Lj}(t - (x_j - x_1)/\bar{v}). \tag{2}$$

The wind speed preview v_{0L} is filtered by a low-pass filter, and the time delay introduced by the filter has to be considered as explained in the next subsection.

3.3. Feedforward Controller

The feedforward controller (see Figure 3a) is based on the work in [8] and combines the baseline feedback controller with a feedforward pitch rate update. The main control goal of the collective pitch feedback controller Σ_{FB} is to maintain the rated rotor speed Ω_{rated} by adjusting the demanded pitch angle θ_c. A wind field $\mathcal{V}$ evolves to v_0 on its way to the turbine and disturbs the system Σ. The measurement of the wind field in front of the turbine by a LIDAR system Σ_L yields v_{0L}. The disturbance could be perfectly compensated by a feedforward controller

$$\Sigma_{FF} = -\Sigma_{\Omega\theta_c}^{-1}\, \Sigma_{\Omega v_0}\, \Sigma_E\, \Sigma_L^{-1}, \tag{3}$$

(a) Feedforward control scheme.　　　　　(b) Static pitch rate curve of the CART2.

Figure 3. The feedforward controller.

if the complete system was known and $\Sigma_{\Omega\theta_c}$ as well as Σ_L were invertible. Due to its complexity, the inversion of $\Sigma_{\Omega\theta_c}$ cannot be found for an aeroelastic model. Here, the stationary pitch curve $\theta_{ss}(v_{ss})$ is used to substitute $-\Sigma_{\Omega\theta_c}^{-1}\Sigma_{\Omega v_0}$. For real applications, it is beneficial to use a pitch rate update $\dot{\theta}_{\mathrm{FF}}$ instead of θ_{FF}:

$$\dot{\theta}_{\mathrm{FF}} = \dot{v}_0 \frac{d\theta_{ss}}{dv_{ss}}(v_0). \tag{4}$$

Figure 3b shows the air density corrected static pitch rate curve $d\theta_{ss}/dv_{ss}$ for the CART2, limited to $3\,\mathrm{deg}/(\mathrm{m/s})$, to avoid high pitch rate near the rated wind speed (see [8]).

　　Further simplifications have to be made for $\Sigma_E\,\Sigma_L^{-1}$, because information is lost by the LIDAR measurement due to the spacial averaging and thus Σ_L cannot be inverted. Also Σ_E is quite complex to model. However, the transfer function G_{LR} from the LIDAR estimate of the wind speed to the rotor effective wind speed can be estimated from measured data via the auto correlation spectrum of the measured wind speed S_{LL} and the cross correlation spectrum S_{SL} between the measured and the rotor effective wind speed. Due to its low pass behavior and the preview provided by the LIDAR, the transfer function can be approximated by a second-order low pass Butterworth filter G_{filter} and a time delay [9]:

$$G_{LR} = \frac{S_{LR}}{S_{LL}} \approx G_{\mathrm{filter}}(s)\,e^{T_{\mathrm{buffer}}s}. \tag{5}$$

Due to the spectral properties of the wind, the G_{LR} is a function of the wavenumber k. The filter is parametrized by a cut-off frequency $f_{\mathrm{cutoff}} = \hat{k}\bar{v}/(2\pi)$, where $\hat{k}$ is the maximum coherent wavenumber (defined at $-3\,\mathrm{dB} \approx 0.7$ below the static value).

　　The time delay is obtained from the following considerations: With Taylor's hypothesis, the wind needs the time $x_1/\bar{v}$ to evolve from the first focus distance to the turbine. Due to the averaging over the full trajectory, v_{0L} is already delayed by $T_{\mathrm{scan}}/2$. The filter delay is approximated by T_{filter}. For using the filtered wind in the feedforward controller (4) instead of v_0, the signal has to be synchronized with v_0 reaching the rotor plane. Therefore the necessary time delay is

$$T_{\mathrm{buffer}} = \frac{x_1}{\bar{v}} - \frac{1}{2}T_{\mathrm{scan}} - T_{\mathrm{filter}} - \tau. \tag{6}$$

The time τ can be used to compensates for the slow down of the wind due to the higher pressure in front of the turbine or small errors in the model reduction (see [3]). Both T_{buffer} and f_{cutoff} are continuously adapted to the mean wind speed $\bar{v}$.

4. Correlation Study

This section describes, how the maximum coherent wavenumber $\hat{k}$ and the prediction time τ for the adaptive filter and the timing of the signal were identified before applying the feedforward control. For this purpose, the measured rotor effective wind speed v_{0L} from the LIDAR is compared to an estimate from turbine data. In the beginning of the campaign the correlation decayed due to the collision of the laser beam with hard targets. This problem could be solved during the campaign by improved data processing.

4.1. Estimator for the Rotor Effective Wind Speed

The rotor effective wind speed v_0 is obtained from simulated turbine data by an estimator similar to the one presented in [14]. Here, the CART2 is modeled by

$$J\dot{\Omega} + M_{LSS} = M_a, \tag{7}$$

where M_a is the aerodynamic torque, M_{LSS} is the low-speed shaft torque, and J is the overall sum of the moments of inertia about the rotation axis.

Moreover, the aerodynamic torque acting on the rotor with radius R is:

$$M_a = \frac{1}{2}\rho\pi R^3 \frac{c_P(\lambda, \theta)}{\lambda} v_0^2 \tag{8}$$

where ρ is the air density, λ is the tip-speed ratio

$$\lambda = \frac{\Omega R}{v_0}, \tag{9}$$

and c_P is the effective power coefficient, obtained from steady-state simulation [15].

With measured data of Ω and M_{LSS} the aerodynamic torque M_a can be calculated using (7). Due to numerical issues (8) is reorganized in a cubic equation in λ:

$$\lambda^3 = \frac{1}{2}\rho\pi R^5 \frac{c_P(\lambda, \theta)}{M_a}\Omega^2. \tag{10}$$

Because of the λ-dependency of c_P, an explicit expression cannot be found. The equation is solved with a set of M_a, Ω and θ, and a three-dimensional look-up table $v_0(M_a, \Omega, \theta)$ is generated, which can then be used to get a time series of v_0 by a three-dimensional interpolation.

### 4.2. Identification of the Filter Parameter

Before applying the LIDAR feedforward update to the CART2, the maximum coherent wavenumber $\hat{k}$ and the prediction time τ have been identified based on the LIDAR and CART2 data of Block 0 using the "BangBang" scanning mode, (see Table 1 and Figure 4).

Figure 5 depicts the measured transfer functions between the v_0 and the wind speeds v_{0Li} from the different measurement distances (solid) as well as the transfer function between v_0 and v_{0L} which is a combination of all measurement distances (dotted). The figure shows, that on the one hand all distances used alone would require more filtering as the combination, while the first and the last distance have the lowest $\hat{k}$. This motivates the use of pulsed systems, because the averaged signal over several focus distances requires less filtering and thus smaller time delays. On the other hand the figure shows the chosen filter. The maximum coherent wavenumber was identified with $\hat{k} = 0.06\,\text{rad/m}$. This is close to the expected value based on an analytic correlation model [16].

Based on the measured cross correlation in Figure 6 between v_0 and the wind speeds v_{0Li}, the preview time was adjusted with $\tau = -0.6\,\text{s}$ in such a way, that predicted previews met the measured ones. The Figure also shows, that the second distance is the best correlated in terms of the peak cross correlation which is equal to the cross correlation coefficient of the synchronized signals. Again, the combination of all distances improves the correlation.

Table 1. Overview of evaluated data.

Block ID	Start Time	End Time	FFoff-sections	FFon-sections high	FFon-sections low	$\hat{k}$ [rad/m]	Yaw [deg]	Scan mode
0	03-30 15:05:47	03-30 15:15:47	0	0	0	0.06	246	BangBang
1	04-13 15:39:29	04-13 16:34:29	8	0	0	<0.01	307	BangBang
2	05-17 01:18:28	05-17 01:28:28	0	0	6	0.02	296	StartStop
3	06-05 23:20:59	06-05 23:30:59	0	6	0	0.06	148	BangBang
4a	07-25 04:06:12	07-25 04:11:12	5	3	0	0.06	250	BangBang
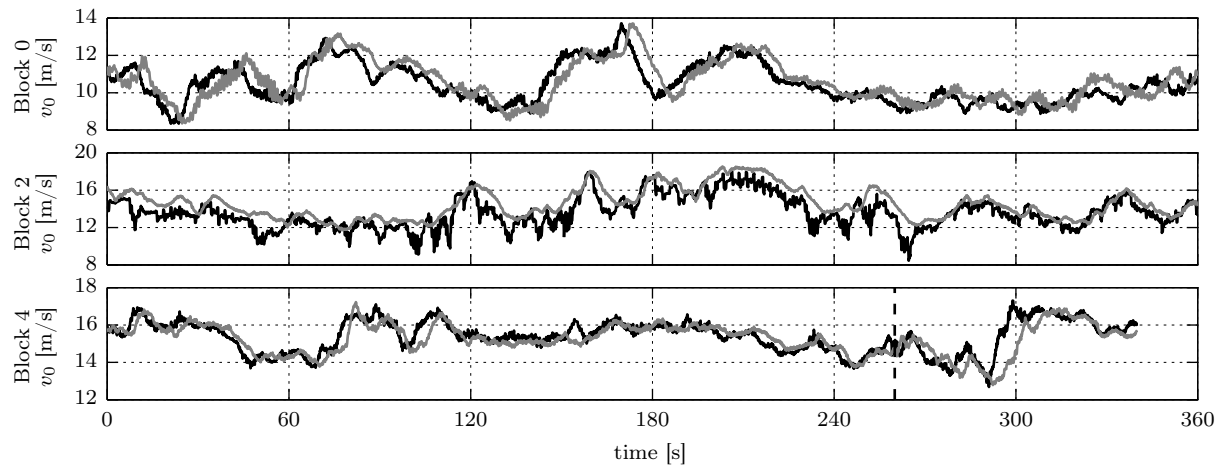
Figure 4. Rotor effective wind speed estimates from the turbine (gray) and the LIDAR (black).
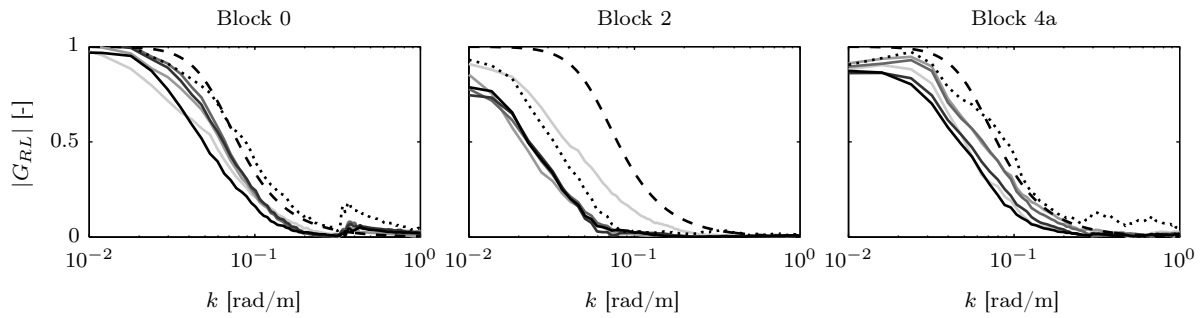
Figure 5. Transfer function between the turbine and the first distance (light gray) to the last (black) and compared to the average v_{0L} (dotted). The dashed line shows to used filter.
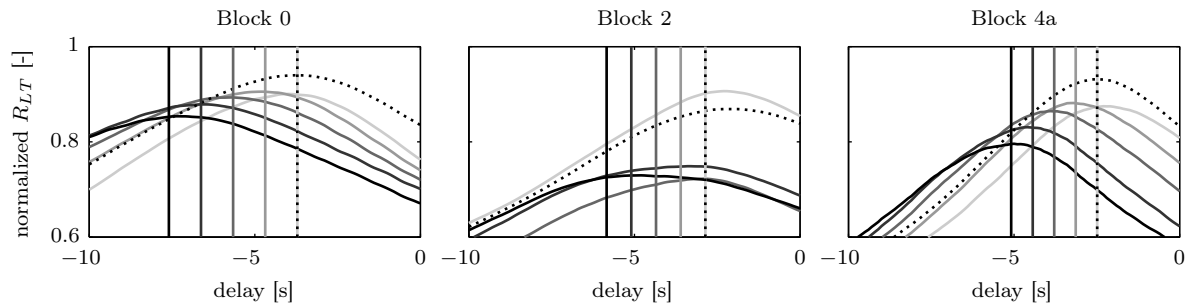
Figure 6. Cross correlation between the turbine and LIDAR: the first distance (light gray) to the last (black) and the average v_{0L} (dotted). The lines indicate the predicted preview.

4.3. Hard Target Problem

During the next period of high wind speeds (Block 1), a lower correlation was discovered ($\hat{k} < 0.01$ rad/m) and the feedforward controller was not applied. A detailed investigation of the data revealed values of v_{los} around 0 m/s, typical for an impact with a hard target. It was assumed due to the position in the trajectory (see Figure 7b) and the yaw dependency, that the met mast and the guy wires were responsible. Figure 7a shows exemplary the v_{los} data distribution over the CNR of a 10 min raw data file. Impact with the rotating blades can easily identified by a lower CNR limit, depending on the trajectory, the number of averaged shoots, and the aerosol concentration. Here -18 dB was used. This cannot be done for the hard target issue, because the CNR value are distributed along the CNR range of the normally reliable data. Due to the high occurrence of this issue, using only data with high v_{los} was not considered. Instead, two strategies were used:

(i) Use the "StartStop" mode and remove all data online with a CNR value above -5 dB, because it was assumed that with this modification the probability of an impact can be minimized and the CNR will be maximized in the case of an impact. This implies that the correlation is supposed to be lower due to the slower trajectory.

(ii) Cut off the FFT spectra at bin 15. The peak detection algorithm is than able to find the second minor peak, see 7c. This implies that v_{los} below 6 m/s cannot be detected.

The first approach was applied in Block 2 with enabled feedforward controller (see Figure 4) without significant improvements. With the second approach the hard target problem was not observed in the rest of the campaign, independent on the yaw direction. For Block 3 and 4a (until 260 s) again a maximum coherent wavenumber close to $\hat{k} = 0.06$ rad/m and a prediction time $\tau = -0.6$ s could be detected and the transfer function as well as the cross correlation show a similar behavior compared to Block 0, see Figure 5 and 6. But at $t \approx 300$ s the LIDAR detects the gust with a higher preview. The average wind speed $\bar{v}$ is calculated by a moving average over 180 s. Further studies are necessary to investigate, if the problem detected in Figure 4 can be improved by a shorter average time. The integral time scale may be a good approach.

Due to problems with the data acquisition system of the turbine and the low wind season, no more than the 4 blocks of significant data were collected during the campaign. For the further analysis the data with positive pitch angles from Block 1 to 4 are divided in sections of 32 s with the feedforward controller on with high and low correlation (FFon high/low) and sections when only the feedback controller was running (FFoff).
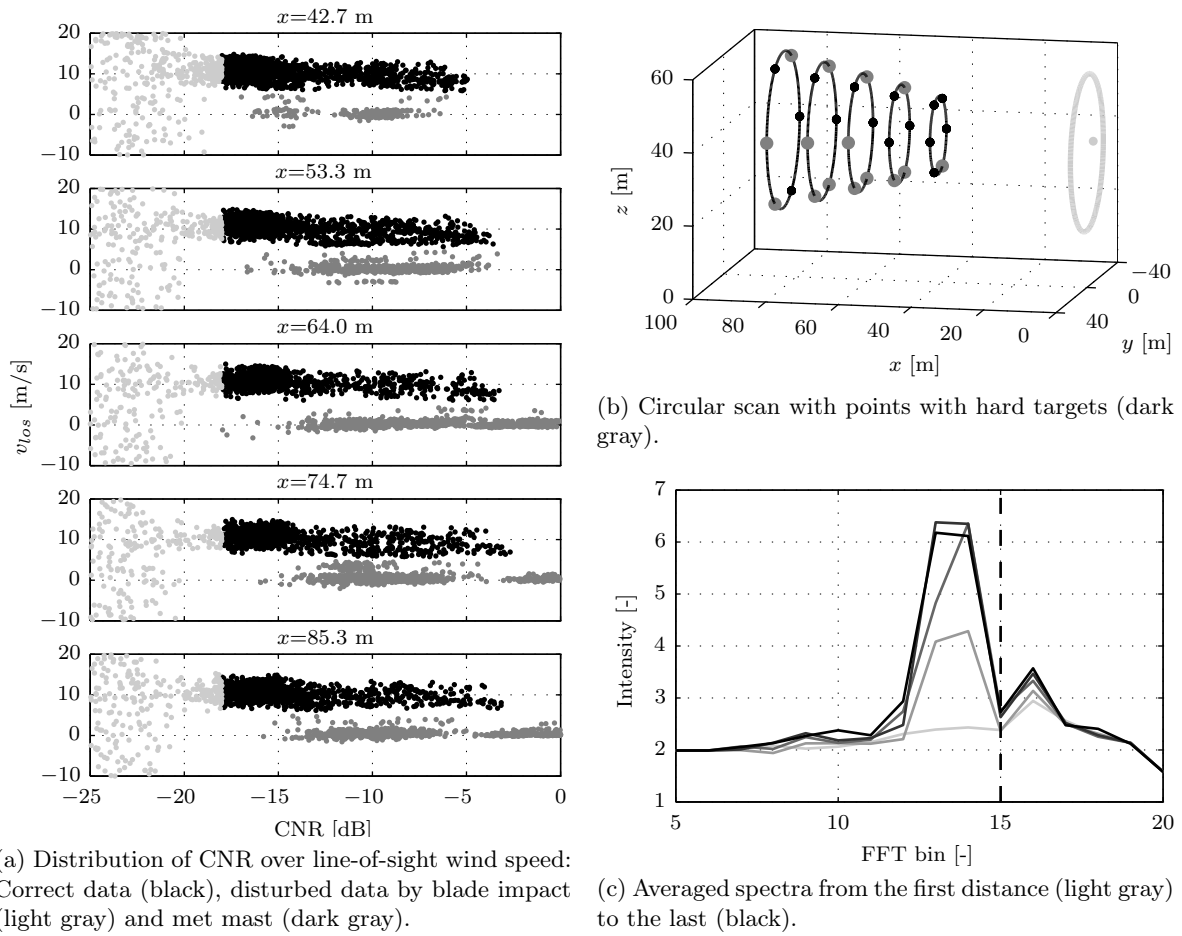
5. Results

The results of the campaign are first examined in the time dome and then evaluated by spectral analysis. Then, the data from turbine and data are used to re-simulate the situation to check, if better results would have been possible by tuning the filter and the feedback controller.
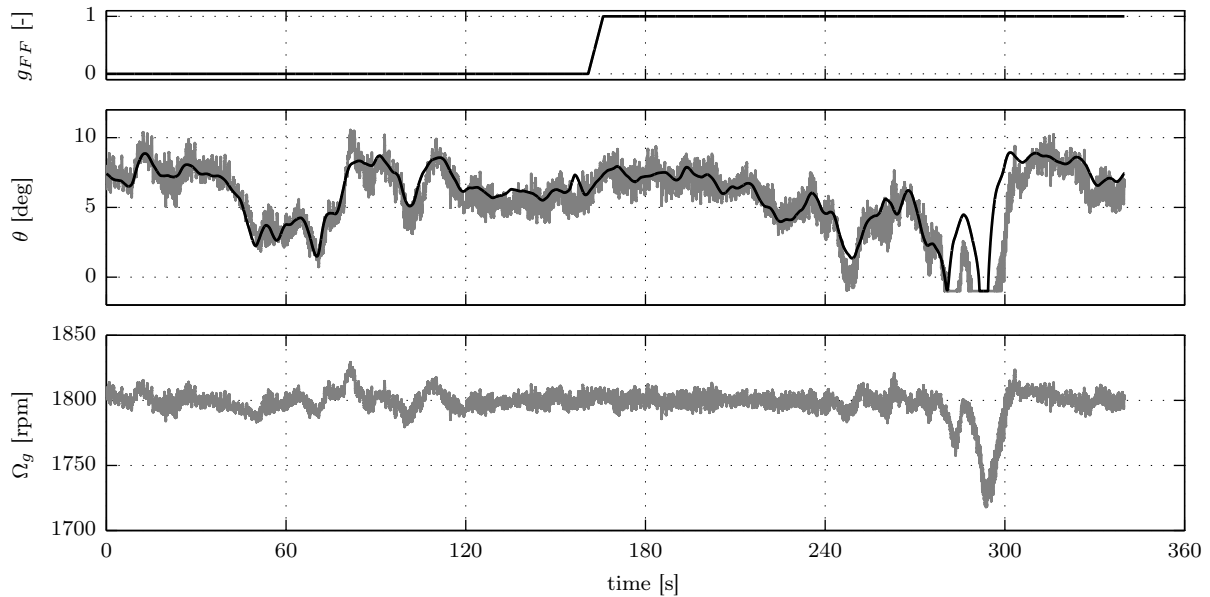
5.1. Time domain

Figure 8 shows the smooth enabling of the feedforward controller by changing the FF switch g_{FF} from 0 to 1, which is multiplied with the pitch rate update $\dot{\theta}_{FF}$. Some reduction of the generator speed can be observed and the pitch angle follows the feedforward pitch angle θ_{FF} for most of the time. As described above, the LIDAR detects the gust at $t \approx 300$ s too early. However, in this case might have been beneficial to avoid a generator speed overshoot when reaching rated speed. This shows, that further investigation is also necessary to improve the feedforward control close to rated wind speed.

Besides the primary control goal to reduce the standard deviation of the generator speed, also some general loads of the turbine, namely the flapwise root bending moment of the first blade M_{flp1} and the tower base bending moment M_T are evaluated and the results are shown in Table

(a) Distribution of CNR over line-of-sight wind speed: Correct data (black), disturbed data by blade impact (light gray) and met mast (dark gray).

(b) Circular scan with points with hard targets (dark gray).

(c) Averaged spectra from the first distance (light gray) to the last (black).

Figure 7. The hard target problem during Block 1.

Figure 8. FF switch, the measured pitch angle (gray) and the feedforward pitch angle (black) and the generator speed for Block 4.

	$\sigma(\Omega_g)$ [rpm]	$\mathrm{DEL}(M_T)$ [kNm]	$\mathrm{DEL}(M_{flp1})$ [Nm]
FFoff	6.89	4.85	435
FFon high	4.74	4.38	380
FFon low	8.77	5.79	404

Table 2. Standard deviation of the generator speed and DEL for tower base bending moment and flapwise blade root bending moment.
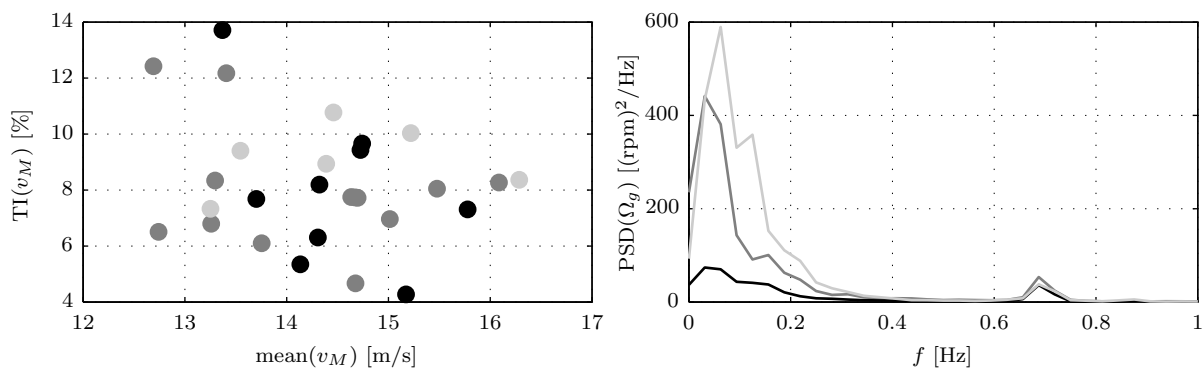

Figure 9. Distribution of turbulence intensity over mean wind speed (left) and PSD of generator speed (right): FFoff(dark gray), FFon high (black), FFon low (light gray).

2. Damage Equivalent Loads (DEL) are calculated based on a rainflow counting with reference number of cycles $2*10^6$ for 20 years lifetime and with a Wöhler exponent of 4 and 10, typical for steel and composite material. For the sections with high correlation the feedforward controller is able to reduce the standard deviation of the generator speed by circa 30 % and the tower loads by 10 %. However, for the sections with low correlation the feedforward controller increases the standard deviation of the generator speed by circa 30 % and the tower loads by circa 20 %. The blades loads are reduced in both cases by circa 10 %. Although the collected data yields only a limited evaluable amount of data, the shown results are considered to be still indicative because the wind conditions of the evaluated sections are comparable. As shown in Figure 9, the turbulence intensities measured by the met mast are distributed over the mean wind speed similarly for the evaluated sections. Further findings can be gathered by the frequency analysis in the next subsection.

5.2. Frequency domain

Figure 9 shows the power spectral density (PSD) of the generator speed for the different cases. Due to the linear scale the area below the PSD corresponds to the square of the standard deviation. In the case of high correlation lower standard deviation is obtained by a reduction of the PSD at low frequencies, e.g. the peak at the 1P-frequency (0.695 Hz, once per revolution) is not affected by the feedforward controller. The PSD of the FFon case with low correlation starts to be above the PSD of the FFoff case at frequencies of 0.0625 Hz which corresponds at a mean wind speed of $\bar{v} = 14\,\mathrm{m/s}$ to a wavenumber of 0.028 rad/m. This value is above the maximum coherent wavenumber $\hat{k} = 0.02\,\mathrm{rad/m}$. Therefore, the increment of the generator speed variations is caused by wrong pitch action of the feedforward controller due to the uncorrelated wind speed measurements.

The PSD of the tower base bending moment M_T and flapwise blade root bending moment
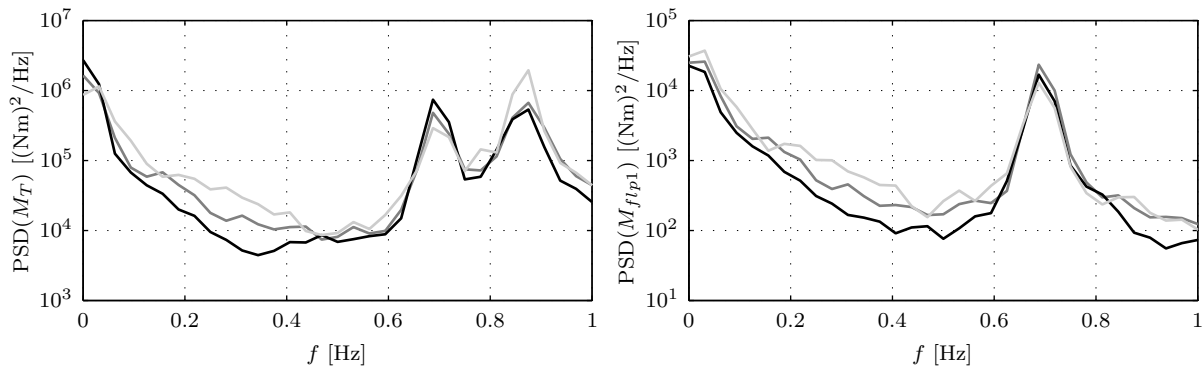
Figure 10. PSD of tower base bending moment and flapwise blade root bending moment: FFoff(dark gray), high FFon (black), low FFon (light gray).

M_{flp1} are illustrated in Figure 10. Although the data base is small, some general observations fit to the considerations above: The PSD again is mainly affected by the feedforward controller at low frequencies: For high correlated LIDAR measurement the PSD is decreased and for low correlation the PSD is above the FFoff case.

5.3. Hybrid Simulations

To results above showed, that the LIDAR assisted feedforward controller was only able to improve the control performance in the case, that the correlation between the LIDAR measurement and the turbine's reaction corresponded to the correlation which was predicted and used in the filter design. For following simulation study investigates, if the used filter was close to the optimum and if further improvements could have be achieved by re-tuning of the feedback controller like proposed in [8, 17]. The first 300 s of the rotor effective wind speed v_0 and the lidar estimate v_{0L} from Block 4 (see Figure 4) is used for the hybrid simulation technique introduced in [18]. An aero-elastic wind turbine model of the CART2 is disturbed by v_0 used as a coherent hub height wind speed. The turbine is controlled by the same feedback controller and in the case of no further changes, the simulation produces a similar reaction of the turbine, because the estimation described in Section 4.1 is based on an inversion of the reduced model.

In a first step, the simulation is repeated with the feedforword controller and different values for the maximum coherent wavenumber $\hat{k}$ and the prediction time τ. 10 values are equally distributed between 0.03 rad/m and 0.12 rad/m for $\hat{k}$ and 13 values between -1.2 s and 1.2 s for τ, resulting in 130 simulations. The top part of Figure 11 shows, that the parameters used in the field testing (black marker) are close to the optimal values for the reduction of the generator speed standard deviation $\sigma(\Omega_g)$. However, for the DEL of the tower base bending moment M_T and the flapwise blade root bending moment M_{flp1} more load reduction is achieved in simulations with larger prediction times and less filtering (higher $\hat{k}$). Similar effect has been reported in [3].

In a second step, the 130 simulations are repeated with a relaxed feedback controller. Both, the proportional and the integral gain are reduced by 1/3 based on the experience gathered in [8]. The lower part of Figure 11 depicts, that on the one hand, the loads can be further reduced at the cost of higher standard deviation of the generator speed. On the other hand the shape of the relative improvement of $\sigma(\Omega_g)$ over the parameters $\hat{k}$ and τ is similar for the combination with the baseline and the re-tuned feedback controller. This confirms the measurement problem ("How can we obtain a signal similar to the rotor effective wind speed from the LIDAR measurements?") and the control problem ("How can we improve the control performance knowing the rotor effective wind speed?") of LIDAR-assisted control can be solved independent from each other: The
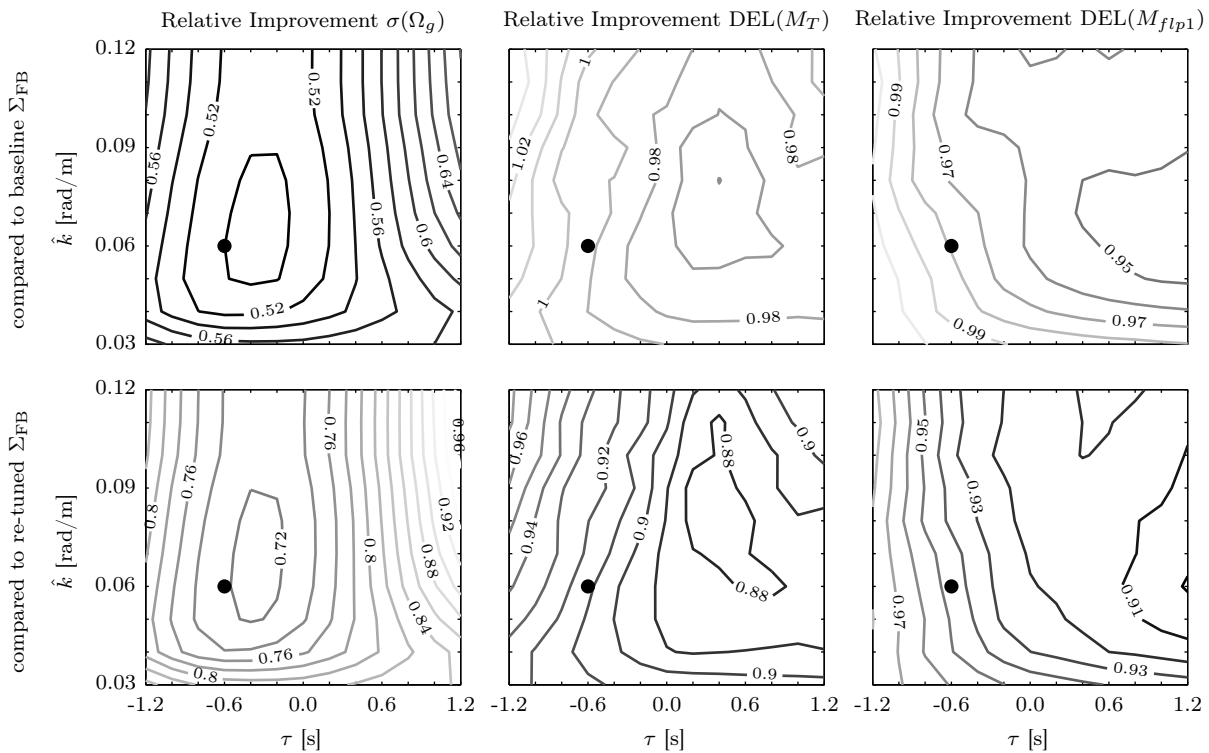
Figure 11. Results from simulation study using v_0 and v_{0L} of Block 4 and aero-elastic CART2 model: Relative improvement with different feedforward parameters over baseline (top) and re-tuned (bottom) feedback controller. Black marker: used parameters in field testing.

adaptive filter is solving the measurement problem best, if it is fitted to the current correlation between LIDAR and turbine's reaction. This is not affected by re-tuning the feedback controller.

6. Conclusions and Outlook

The beneficial effect of LIDAR-assisted control for wind turbines in simulations have been reported in several publications in recent time. This work shows this can be achieved also under real conditions. In a field testing campaign a scanning LIDAR systems has been integrated in a control systems and was able to improved collective pitch control.

　　Although only few data could be collected, the data proofs that it is important to filter the data according to the correlation of the turbine and the LIDAR system. In the case of low correlation, which was due to the initially not considered impact with the met mast and guy wires, the feedforward controller was not beneficial to the turbine. During the campaign a method presented in this paper was developed to avoid the decay of measurement quality due to the hard targets. In the case of high correlation, the standard deviation of the rotor speed has been reduced by 30 % and 10 % lower structural loads on the tower base have been observed.

　　Furthermore, a simulation study using the simultaneously measured turbine and LIDAR data confirms, that the filter fitted to correlation yield the best results and that loads can be further reduced by relaxing the feedback controller independent from the filter design.

Acknowledgments

References

[1] M. Harris, M. Hand, and A. Writght, "Lidar for turbine control," *Technical Report NREL/TP-500-39154*, 2006.

[2] J. Laks, L. Y. Pao, A. Wright, N. Kelley, and B. Jonkman, "Blade pitch control with preview wind measurements," in *Proceedings of the 48th AIAA Aerospace Sciences Meeting Including the New Horizons Forum and Aerospace Exposition*, Orlando, USA, 2010.

[3] F. Dunne, D. Schlipf, L. Y. Pao, A. D. Wright, B. Jonkman, N. Kelley, and E. Simley, "Comparison of two independent lidar-based pitch control designs," in *Proc. 50th AIAA Aerospace Sciences Meeting Including the New Horizons Forum and Aerospace Exposition*, 2012.

[4] D. Schlipf, D. J. Schlipf, and M. Kühn, "Nonlinear model predictive control of wind turbines using LIDAR," *Wind Energy*, vol. 16, no. 7, pp. 1107–1129, 2013.

[5] A. Körber and R. King, "Nonlinear model predictive control for wind turbines," in *Proceedings of the European Wind Energy Association Annual event*, Brussels, Belgium, 2011.

[6] L. C. Henriksen, "Model predictive control of wind turbines," Ph.D. dissertation, Technical University of Denmark, 2011.

[7] K. A. Kragh, M. H. Hansen, and T. Mikkelsen, "Precision and shortcomings of yaw error estimation using spinner-based light detection and ranging," *Wind Energy*, 2012.

[8] D. Schlipf, T. Fischer, C. E. Carcangiu, M. Rossetti, and E. Bossanyi, "Load analysis of look-ahead collective pitch control using LiDAR," in *Proceedings of the German Wind Energy Conference DEWEK*, Bremen, Germany, 2010.

[9] D. Schlipf and P. W. Cheng, "Adaptive feed forward control for wind turbines," *at - Automatisierungstechnik*, vol. 61, no. 5, pp. 329–338, 2013.

[10] E. Bossanyi, A. Wright, and P. Fleming, "Controller field test on the NREL CART2 turbine," NREL, Tech. Rep. NREL/TP-5000-49085, December 2010.

[11] A. Rettenmeier, O. Bischoff, M. Hofsäß, D. Schlipf, J. J. Trujillo, and M. Kühn, "Wind field analysis using a nacelle-based lidar system," in *Presentation at the European Wind Energy Conference*, Warsaw, Poland, 2010.

[12] K. Johnson, L. J. Fingersh, and A. Wright, "Controls advanced research turbine: Lessons learned during advanced controls testing," NREL, Tech. Rep. NREL/TP-500-38130, June 2005.

[13] A. D. Wright, P. Fleming, and J. W. van Wingerden, "Refinements and tests of an advanced controller to mitigate fatigue loads in the controls advanced research turbine," in *Proceedings of the 49th AIAA Aerospace Sciences Meeting Including the New Horizons Forum and Aerospace Exposition*, Orlando, USA, 2011.

[14] E. van der Hooft and T. G. van Engelen, "Estimated wind speed feed forward control for wind turbine operation optimization," in *European Wind Energy Conference*, London, GB, 2004.

[15] M. L. Buhl, "WT_Perf user's guide," NREL, Tech. Rep. NREL/TP-500-41136, April 2004.

[16] D. Schlipf, J. Mann, and P. W. Cheng, "Model of the correlation between lidar systems and wind turbines for lidar assisted control," *Journal of Atmospheric and Oceanic Technology*, vol. 30, no. 10, pp. 2233–2240, 2013.

[17] E. Bossanyi, "Un-freezing the turbulence: improved wind field modelling for investigating lidar-assisted wind turbine control," in *Proceedings of the EWEA Annual event*, Copenhagen, Denmark, 2012.

[18] D. Schlipf, P. Fleming, S. Kapp, A. Scholbrock, F. Haizmann, F. Belen, A. Wright, and P. W. Cheng, "Direct speed control using lidar and turbine data," in *Proceedings of the American Control Conference*, Washington, USA, 2013.